# $CO_2$ as a soft oxidant for propane oxidative dehydrogenation: a mechanistic study using *operando* UV Raman spectroscopy

Simone Rogg, Christian Hess*

Eduard-Zintl-Institut für Anorganische und Physikalische Chemie, Technische Universität Darmstadt, Alarich-Weiss-Str. 8, 64287 Darmstadt, Germany

*Corresponding Author (E-mail: christian.hess@tu-darmstadt.de)

**Abstract**

The utilization of $CO_2$ as an oxidant has recently attracted increasing attention due to its mild oxidizing properties allowing higher product selectivities to be achieved e.g. in propane oxidative dehydrogenation (ODH). In this communication we address mechanistic aspects of propane ODH over silica supported vanadia ($VO_x/SiO_2$) catalysts in the presence of $CO_2$ as oxidizing agent. The use of *operando* UV Raman spectroscopy reveals distinct changes in the surface vanadia structure including breakage of V-O-V bonds and a partial reduction of vanadyl, as well as the formation of support hydroxyl groups, while the presence of $CO_2$ is observed to prevent coke deposition. Our results are fully consistent with the occurrence of two parallel pathways, i.e., direct ODH (one step) and dehydrogenation followed by a reverse water-gas shift reaction (two step), supporting previous literature proposals.

**Keywords**

Propylene, oxidative dehydrogenation (ODH), $CO_2$, reverse water-gas shift, supported metal oxide, vanadia, *operando* Raman, reaction mechanism

## 1. Introduction

The worldwide demand for olefins is growing as they are considered key components of the chemical industry. [1,2] Currently, the main processes for olefin production are steam cracking, fluid-catalytic-cracking (FCC), and catalytic dehydrogenation (DH). It has been predicted that the supply from refinery FCC and steam-crackers will not cover future demand. Nowadays, DH as an economically attractive technology fills the gap. [1] The oxidative dehydrogenation (ODH) is an energy-saving alternative to these technologies. Molecular oxygen effectively suppresses coke formation, which is a major obstacle in DH, but only low propene selectivities are obtained. Thus, the industrial implementation, e.g. of propane ODH, is still hampered owing to low propylene yields. [2,3] More recently, the potential of carbon capture and utilization (CCU) has been evaluated towards the problems of greenhouse-gas emissions and the increasing energy demand [4–6] e.g. by employing carbon dioxide ($CO_2$) as a carbon source.

In the context of high-temperature ODH reactions, $CO_2$ has received considerable attention as a mild oxidant, preventing deep oxidation thereby increasing olefin selectivities. [7–12] Hence the use of $CO_2$ as an oxidant in ODH is attractive due to its abundance but suffers from its chemical inertness. [7,9,10,13] Previous studies have shown that supported transition metal oxides like chromia [14–20], gallium oxide [14], vanadia [21–25], as well as ceria-based systems [25,26] are catalytically active in propane ODH with $CO_2$. The respective catalytic activity shows a strong dependency on the nature of the support. Michorczyk et al. systematically compared the activity of chromia deposited on different silica supports like conventional $SiO_2$, hexagonal SBA-15, and cubic SBA-1 in the presence and absence of $CO_2$. [17] In a subsequent study, the influence of chromium content deposited on SBA-1 was investigated in more detail. [18] For a loading of 7 wt. % Cr, a maximum conversion of 37.7 % and a selectivity of 85.0 % was reported at 550 °C. *In situ* UV-Vis measurements performed during $CO_2$ ODH provided insights into the redox behavior of the present Cr species, allowing for a mechanistic discussion of possible oxidative and nonoxidative pathways, showing that

$Cr^{6+}$ species were rapidly reduced to $Cr^{3+}/Cr^{2+}$. The authors proposed chromia in its oxidized state to operate in ODH, and reduced Cr sites to be responsible for nonoxidative dehydrogenation of propane.

More recently, Ascoop et al. studied the ODH of propane over $WO_x$-$VO_x/SiO_2$ catalysts, [27] both experimentally and theoretically, and proposed the reaction to proceed simultaneously via direct ODH and a two-step pathway, including propane dehydrogenation (DH) followed by the reverse-water gas shift reaction (rWGS). Nevertheless, owing to its complexity, the role of $CO_2$ in ODH reactions and, in particular, its influence on the structural dynamics of the catalyst is largely unexplored. To further enhance the mechanistic understanding and to develop structure-activity relationships as a basis for a rational catalyst design, *operando* methods have been widely applied to ODH reactions. [28–35] Recently, we have employed UV resonance Raman spectroscopy to elucidate the structural dynamics of supported vanadia catalysts during ethanol and propane ODH, demonstrating the high sensitivity of the technique for detailed catalyst and adsorbate characterization. [33–35] The possibilities and limits of UV Raman spectroscopy in the context of heterogeneous catalysis have previously been discussed in reviews. [36–38]

In this communication, we address mechanistic aspects of propane ODH over silica supported vanadia ($VO_x/SiO_2$) catalysts using $CO_2$ as oxidizing agent. *Operando* UV resonance Raman spectroscopy is employed in combination with gas chromatography (GC) to elucidate the structural dynamics of the catalyst surface under propane ODH conditions, which is not accessible by visible laser excitation. To gain additional insight into the reaction mechanism, *operando* Raman spectra were also recorded during propane DH and the rWGS reaction. Based on our findings we discuss the role of the oxidizing agent in propane to propylene conversion.

## 2. Experimental

**Catalyst Preparation.** Mesoporous silica SBA-15 was prepared as described previously in detail [39,40], by mixing 4.0 g of Pluronic P123 ($EO_{20}PO_{70}EO_{20}$, BASF) with 120 ml of 2 M HCl and 30 ml deionized water in a polypropylene bottle at 35 °C and subsequent addition of 8.5 g of tetraethyl orthosilicate (TEOS, Sigma-Aldrich, 99%). After heating in an oven at 85 °C for 24 h, the suspension was filtered and calcined at 550°C for 12 h in ambient air by applying a heating ramp of 1.5 °C/min. For vanadium deposition on the silica SBA-15 support, incipient wetness impregnation [41] was employed, by mixing vanadium(V) oxytriisopropoxide (97%, Sigma Aldrich) with anhydrous 2-propanol (99.5%) in a glove box and drop-wise addition of the solution to the support while pulverizing in an agate mortar. Subsequently, the yellow powders were calcined in an oven at 550 °C for 12 h with a heating rate of 1.5 °C/min. This material will be referred to as $VO_x/SiO_2$. For the investigations 200–300 μm sieve fractions were used.

**Catalyst Characterization.** Nitrogen adsorption-desorption experiments were performed on a Nova Station A (Quantachrome Instruments). Prior to the measurements the samples were evacuated for 24 h at 150°C. The specific surface area was determined based on nitrogen adsorption/desorption isotherms by applying the standard multipoint BET (Brunauer-Emmett-Teller) model. Two charges were synthesized exhibiting surface areas of 604 and 617 $m^2/g$, corresponding to a vanadia density of 0.6 $V/nm^2$. Note that the two samples showed no significant differences in their properties.

UV-Vis spectroscopic measurements were performed on a Jasco V-770 UV-vis/NIR spectrometer, employing a halogen and a deuterium lamp for excitation. Spectra were taken within 200-1100 nm at a resolution of 0.5 nm. SBA-15 was used as a white standard.

**Catalytic Tests.** Catalytic tests were performed in a reactor (CCR1000, Linkam Scientific Instruments Ltd.) at temperatures between 320 and 593 °C after dehydrating the catalyst for one hour in helium, by a stepwise increase of the temperature without any re-oxidation steps. Two measurements were performed at each temperature. Specified temperatures are measured

via a thermocouple at the bottom of the sample bed. The ceramic sample holder was loaded with about 15 mg of $VO_x/SiO_2$ sample on a ceramic fiber fleece. The reactor was applied in a fluidized bed mode [42], ensuring constant mixing of the particles from the hotter bottom to the cooler surface. The reaction feed consisted of 12.5% $C_3H_8$/12.5% $CO_2$/He and 12.5% $C_3H_8$/He at a total flow of 40 ml/min. Prior to reactive conditions, the catalysts were dehydrated for one hour. Gas-phase analysis was performed online using an Agilent 7890B Series gas chromatograph. The gas components were separated by two columns, a HP-Plot Q (30m×0.535 mm×40 um) and a CP-Molsieve 5A (25 m×0.53 mm×50 um), which are connected in series, followed by the detection via a thermal conductivity detector (TCD) and a flame ionization detector (FID). The conversion and selectivity were determined based on the detected amounts of reactants and products (see Supporting Information). The carbon deficit was <3.6% for DH and <1% for ODH conditions.

***Operando* Raman Spectroscopy.** Raman spectra were recorded in a backscattering geometry on a triple-stage spectrometer (Princeton Instruments, TriVista 555) equipped with a nitrogen-cooled CCD camera (Princeton Instruments, Spec 10:2kBUV) and calibrated with mercury spectral lamp. The resolution of the spectrometer was 1 $cm^{-1}$. The excitation was performed with 256.7 nm laser radiation using a titanium-sapphire (Ti:Sa) solid state laser (Indigo-S, Coherent) and anisotropic BBO and LBO crystals for frequency multiplication. The laser power was adjusted to 8.8–8.9 mW at the location of the sample. The use of a Linkam cell reactor in fluidized-bed mode prevented potential sample heating and/or damage caused by the UV laser excitation. Details of the Raman spectrometer can be found elsewhere. [33,43] The data was processed via Matlab R2015a, which included background subtraction, smoothing with a moving-average filter, and merging. The fit analysis of the vanadyl feature was performed by using Voigt functions.

For *operando* measurements, the output of the cell reactor was connected to the online gas chromatograph for continuous gas-phase detection. Prior to *operando* experiments a

pretreatment procedure was applied. The catalyst was dehydrated for 1 h at 502 °C under oxidative conditions (12.5% $O_2$/He). Raman spectra were taken after increasing the temperature to 547 °C. After flushing the reactor and tubes with He, the catalyst was reduced with 7.5% $H_2$/Ar and pre-oxidized with either 12.5% $CO_2$/He or 12.5% $O_2$/He. *Operando* conditions consisted of 12.5% $C_3H_8$/12.5% $CO_2$/He. Afterwards, the sample was regenerated under a flow of 12.5% $CO_2$/He. *Operando* conditions for propane DH consisted of 12.5% $C_3H_8$/He and those for the rWGS reaction of 6.5% $H_2$/12.5% $CO_2$/Ar.

## 3. Results and Discussion

Figure 1 depicts the temperature-dependent catalytic performance of the $VO_x/SiO_2$ catalyst in propane dehydrogenation with and without the presence of $CO_2$ at a total flow rate of 40 ml/min. The catalyst shows catalytic activity between 450 and 600 °C with a maximum propane conversion of around 3% for ODH and 5–6% for DH. The larger DH values may be attributed to the higher He concentration in the feed, considering its high thermal conductivity; to this end, a dependence of sample temperature on the presence of the inert (He vs $N_2$) was confirmed in separate experiments. At the above conversion levels, propene selectivities >92% are detected. In order to determine the background activity, the procedure was repeated with an empty reaction cell, resulting in conversions <0.5 % with selectivities <52 %. During DH, ethane, ethylene, and methane were detected besides propylene and $H_2$. The detection of significant amounts of CO during $CO_2$ ODH is a strong indicator for the participation of $CO_2$ in the overall ODH reaction (see SI). As the amount of converted propane exceeded the amount of converted $CO_2$, either propane dehydrogenation occurs in parallel or a two-step pathway with DH followed by the rWGS reaction takes place. As indicated in Figure 1, for the *operando* UV Raman experiments described in the following, a reaction temperature of 547 °C was chosen. Details of the catalytic performance under *operando* conditions are summarized in Table S1.

Figure 2 depicts a series of *in situ/operando* UV Raman spectra (256.7 nm) of the $VO_x/SiO_2$ catalyst at a reaction temperature of 547 °C in different gas atmospheres. As a pretreatment (see experimental section), the catalyst was first dehydrated ($O_2$/He), then reduced ($H_2$/Ar) and finally re-oxidized ($CO_2$/He) to prepare a reproducible reference state of the catalyst for propane ODH with $CO_2$. The *operando* spectrum recorded under reaction conditions shows a distinct spectral signature, which is different to the reduced state ($H_2$/Ar) and the oxidized state ($CO_2$/He). The spectrum recorded after re-oxidation in $CO_2$ ($CO_2$/He, After) resembles that obtained prior to reaction ($CO_2$/He, Prior), indicating that the starting state of the catalyst is largely restored. As a quantitative measure of reduction, analysis of the vanadyl (V=O) feature at 1033 $cm^{-1}$ reveals a decrease in intensity to 42% for reducing ($H_2$/Ar) and to 55% for reaction conditions, as compared to the original state ($O_2$/He). While the assignment of the vibrational features will be discussed in the following, we can state at this point that UV Raman spectroscopy has the sensitivity to detect structural changes of the catalyst as a function of the gas environment. Moreover, each catalyst state is represented by a vibrational signature specific to the applied gas composition.

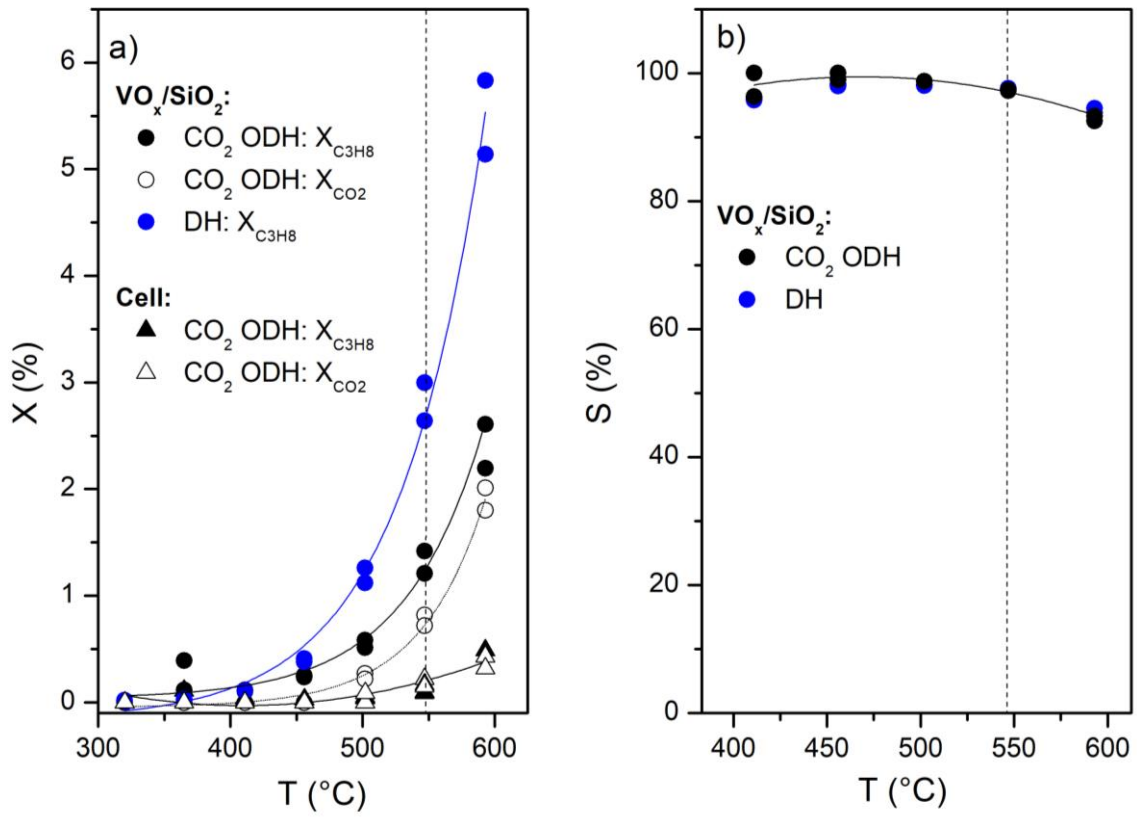


**Figure 1.** Temperature-dependent performance of the $VO_x/SiO_2$ catalyst in propane dehydrogenation with and without the presence of $CO_2$. The gas composition for $CO_2$ ODH consisted of 12.5% $C_3H_8$ / 12.5% $CO_2$ / He, and that for DH of 12.5% $C_3H_8$ / He, both at a total flow of 40 ml/min. a) Temperature-dependent $C_3H_8$ and $CO_2$ conversion of the $VO_x/SiO_2$ and the empty cell during $CO_2$ ODH and DH. b) Temperate-dependent selectivities of the $VO_x/SiO_2$ catalyst during $CO_2$ ODH and DH. Lines are to guide the eye.

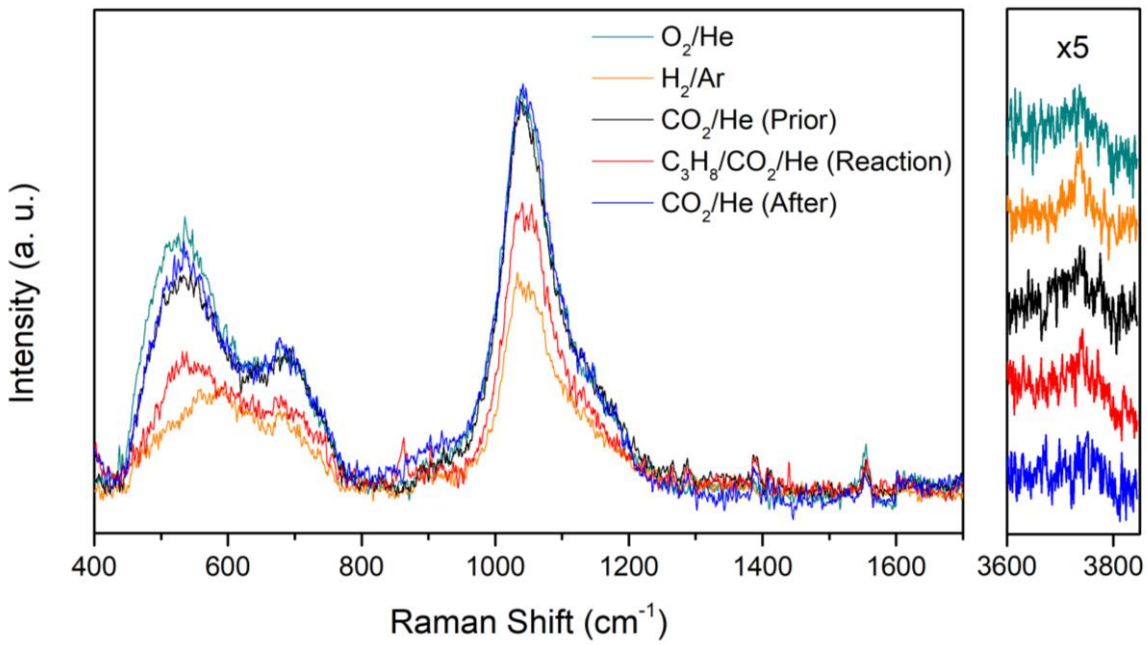


**Figure 2.** *Operando* 256.7 nm Raman spectra of the $VO_x/SiO_2$ catalyst. The experiment included a pretreatment procedure with 7.5% $H_2$ in Ar as described in the text. Reaction conditions consisted of 12.5 % $C_3H_8$/ 12.5 % $CO_2$/ 75 % He. The catalyst was re-oxidized with 12.5 % $CO_2$/ 75 % He before and after the reaction. For better visibility, the hydroxyl region is plotted with an offset.

To analyze the spectral profiles in more detail, Figure 3 shows UV Raman spectra normalized to the vanadyl signal at 1033 $cm^{-1}$ (a) and the signal at 608 $cm^{-1}$ (b). This presentation allows a comparison of different catalyst states under oxidizing ($O_2$ vs $CO_2$) and reducing/reaction ($H_2$ vs $C_3H_8/CO_2$) conditions. As reference for both series, we use the spectrum in $CO_2$/He prior to reaction. In the presence of $CO_2$, typical gas-phase $CO_2$ Raman signals are detected at 1264, 1285, 1388, and 1409 $cm^{-1}$, which originate from a Fermi resonance (1285 and 1388 $cm^{-1}$) and their corresponding hot band features (1264 and 1409 $cm^{-1}$). [44] The Raman signals at around 860 and 2900 $cm^{-1}$ (see Figures 2, 3, and S2) can be attributed to gas-phase propane by comparison with the gas-phase spectrum of propane

measured under the same conditions. The omnipresent signal at 1580 $cm^{-1}$ originates from gas-phase oxygen contributions accumulated outside the *in situ/operando* cell. The region between 1700 and 3600 $cm^{-1}$ is omitted from the following discussion as there are no further signals of relevance for the mechanistic discussion but is shown in the SI (see Figure S2).

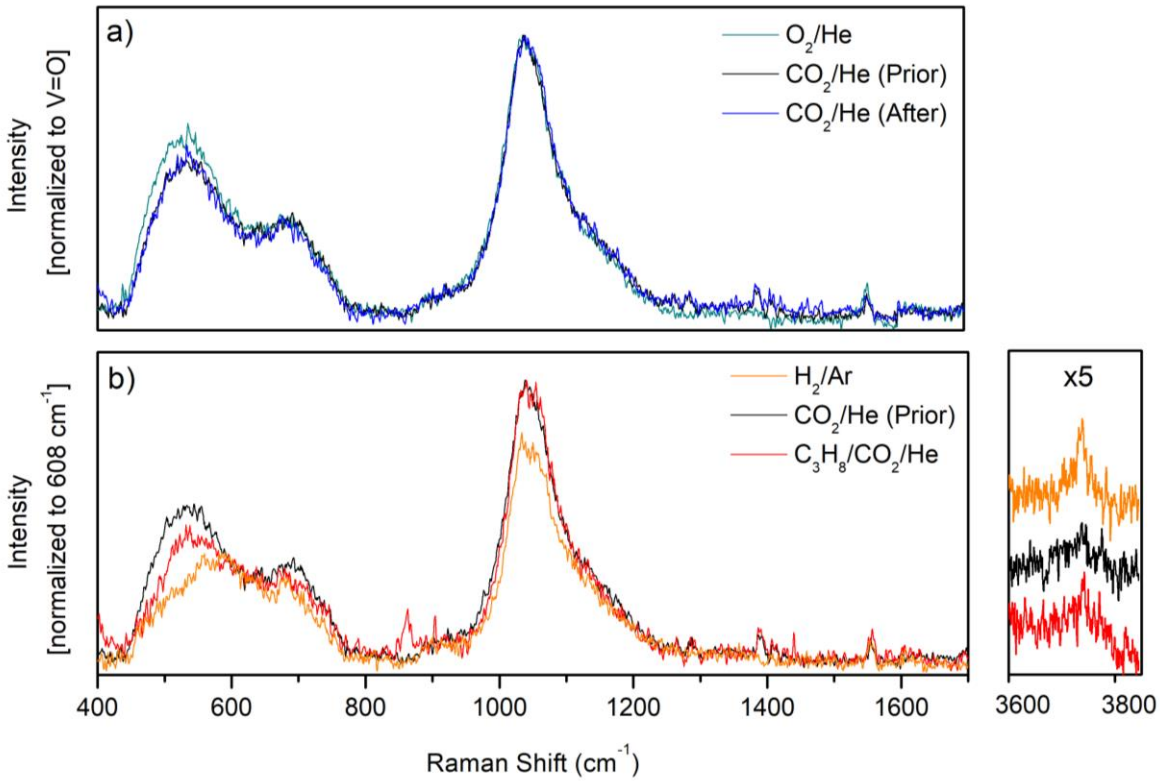


**Figure 3.** *Operando* 256.7 nm Raman spectra of the $VO_x/SiO_2$ catalyst. a) Direct comparison of the dehydrated state with the conditions before and after the reaction. Spectra were normalized to V=O. b) Direct comparison of the hydrogen-reduced state with the Raman spectrum obtained under *operando* conditions. The position of the D2 band of SBA-15 at 608 $cm^{-1}$ was used as a reference point for normalization. For better visibility, the hydroxyl region is plotted with an offset.

The top panel of Figure 3 depicts Raman spectra of the $VO_x/SiO_2$ catalyst in oxidizing gas atmospheres. The spectra are characterized by vanadia-related features at around 550/695,

915 (sh), 1033, and 1150 $cm^{-1}$, which originate from V-O-V, V-O-Si (in phase interphase), V=O, and V-O-M (M = Si, V) (combination) stretching modes, respectively, as reported previously in the literature. [33] More detailed analysis reveals that there are additional features at around 465 and 1070 $cm^{-1}$, which result from V-O-Si and V-O-Si (out-of-phase interphase) stretching, respectively, as discussed in detail before. [45] As a result of UV laser excitation at 256.7 nm, surface vanadia-related features are resonantly enhanced in comparison to the silica support, significantly increasing the sensitivity of Raman spectroscopy towards structural analysis of the surface vanadia species. From the UV Raman analysis in combination with UV-Vis spectra we can conclude that under oxidizing conditions surface vanadia is mainly present as dispersed dimeric/small oligomeric species, while monomers cannot be excluded. Please note that we can rule out the presence of microcrystalline $V_2O_5$ due to the absence of its characteristic signals (e.g. 995 $cm^{-1}$). [46,47]

To allow for a better comparison of the spectral profiles, the spectra in the top panel of Figure 3 were normalized to the vanadyl (V=O) signal, showing good agreement of the vanadia surface structure after oxidation of the catalyst using either $O_2$ or $CO_2$ as oxidizing agent, as probed by UV Raman. Turning to reducing/reaction conditions, the bottom panel of Figure 3 compares the Raman spectrum of the $VO_x/SiO_2$ catalyst in $H_2$/Ar (orange) and $C_3H_8/CO_2$/He (red) atmosphere. During the hydrogen treatment, the catalyst is significantly reduced as indicated by the smaller V=O intensity compared to the $CO_2$/He reference spectrum, while the decreased V-O-V signals at around 550 $cm^{-1}$ and 695 $cm^{-1}$ are indicative of partial V-O-V bond breakage and thus a reduction in the degree of surface vanadia oligomerization. Upon exposure to $H_2$/Ar, an additional feature at 3738 $cm^{-1}$ is observed, which is readily assigned to SiO-H stretching vibrations of isolated surface hydroxyl groups. [33,48] The *operando* Raman spectrum recorded during propane ODH (with $CO_2$) represents an intermediate state between those referenced by the $H_2$/Ar and $CO_2$/He atmospheres. Interestingly, the degree of reduction appears to be related to the intensity of the SiO-H signal, which shows a small but reproducible

dependence on the gas atmosphere. The presence of CO in the outlet gas phase suggests that $CO_2$ is constantly re-oxidizing the catalyst during the reaction. Comparison of the *operando* Raman spectrum to that obtained in $CO_2$/He (here "prior to reaction"), reveals a significant lower intensity within the region 430 - 800 $cm^{-1}$, which corresponds to V-O-V and V-O-Si bonds. These findings are supported by the absence of carbonaceous species, which would be expected at around 1350 and 1600 $cm^{-1}$ [49,50] For additional mechanistic insights also other reactions pathways (DH, rWGS) were investigated using UV Raman spectroscopy as described in the following.

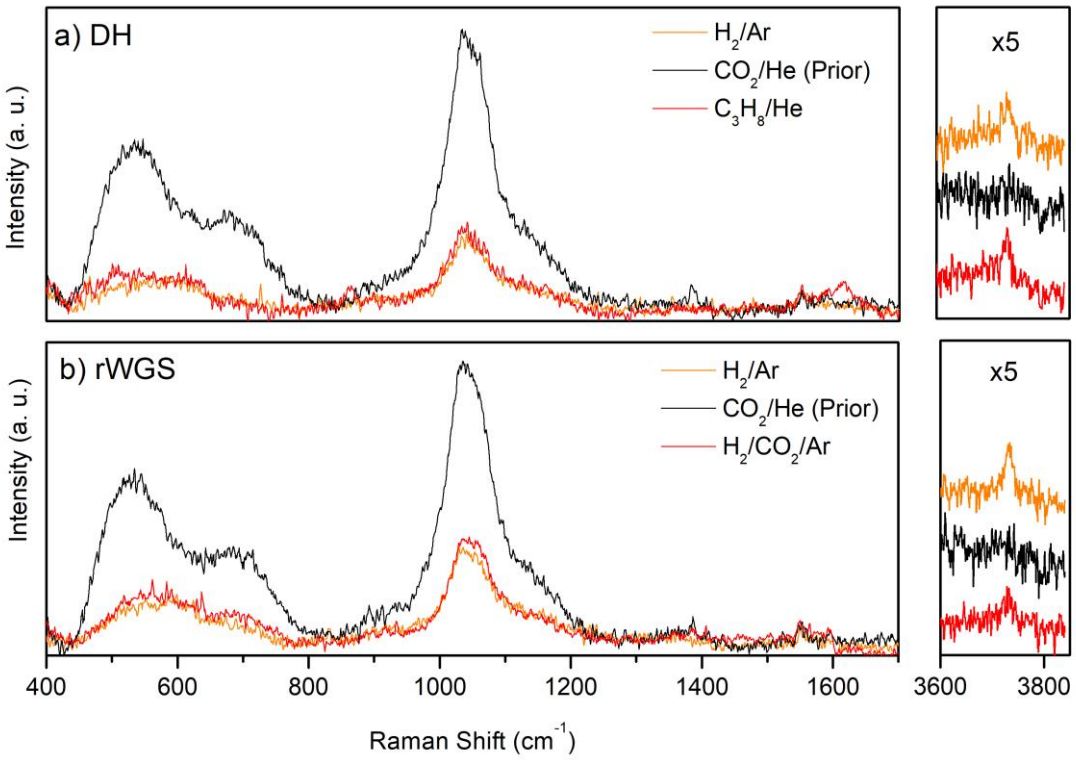


**Figure 4.** *Operando* 256.7 nm Raman spectra of the $VO_x/SiO_2$ catalyst in a) propane DH (12.5 % $C_3H_8$ / 87.5 % He) and b) rWGS (6.5% $H_2$/12.5% $CO_2$/Ar), compared with the hydrogen-reduced and the re-oxidized state.

Figure 4 depicts *operando* UV Raman spectra (256.7 nm) of the $VO_x/SiO_2$ catalyst under DH and rWGS conditions at a reaction temperature of 547 °C. The catalytic performance is summarized in Table S1. Please note that during DH the catalyst turns immediately grey, which would largely prevent an *operando* analysis using visible Raman spectroscopy, in contrast to UV laser excitation. For DH, a higher conversion of propane molecules was observed as in the presence of $CO_2$ (see Figure 1). As shown in the top panel of Figure 4, the *operando* Raman spectrum recorded under DH conditions strongly resembles the hydrogen-reduced state ($H_2$/Ar), indicating that there are no major structural differences between the surface vanadia species. This is confirmed by the comparable vanadyl and hydroxyl signals. In contrast, in the presence of $CO_2$, an intermediate state with structural differences is observed. As expected, under DH conditions, carbon deposits are detected at around 1600 $cm^{-1}$ (see Figure 4).

The rWGS experiment allows the comparison of the hydrogen-reduced state with and without $CO_2$. As shown in the bottom panel of Figure 4, the catalyst adopts an intermediate state under reaction conditions, somewhat similar to the ODH with $CO_2$, which is further confirmed by the SiO-H signal. We therefore conclude that $CO_2$ constantly re-oxidizes the catalyst during the reaction. Based on the relative intensity of the vanadyl signal, the presence of hydrogen leads to a more reducing environment as compared to propane (see Figure 3), which cannot be fully compensated by the presence of $CO_2$.

These complementary *operando* experiments confirm that $CO_2$ participates in the overall reaction network of the propane ODH with $CO_2$. The conversion of propane may proceed via two reaction pathways, i.e., direct ODH (one-step) and DH coupled with a subsequent RWGS reaction (two-step), as the *operando* Raman spectra and the catalytic results are consistent with both channels.

**Mechanistic Discussion.** In the following discussion, besides the role of $CO_2$, we will address the question, whether the overall propane ODH reaction proceeds via a one-step (ODH) and/or

a two-step (DH and RWGS) pathway. The catalytic data confirms that $CO_2$ successfully participated in the overall ODH reaction over the $VO_x/SiO_2$ catalyst. During dehydrogenation without the assistance of $CO_2$, almost no CO was detected. Hence, the observed CO production is related to the activation of $CO_2$. Moreover, the amount of detected $H_2$ was significantly reduced, indicating that either ODH and DH occur in parallel or that the mechanism follows a two-step pathway with a subsequent rWGS reaction.

According to the Raman experiments the hydrogen-reduced state can be related to surface vanadia species with low nuclearity, containing reduced vanadium (3+/4+) and possibly H attached to vanadyl and/or bridging oxygen, i.e., lattice oxygen, and even interface oxygen sites (V-O-Si) (see Figure 5). In the context of re-oxidation with $CO_2$, previous studies by Haija et al. [51] on $CO_2$ adsorption on $V_2O_3(0001)$ via temperature programmed desorption (TPD) and infrared reflection absorption spectroscopy (IRAS) are of interest. Below 200 K, $CO_2$ adsorbed molecularly on vanadyl terminated $V_2O_3(0001)$. Electron irradiation led to the removal of vanadyl oxygen and subsequent binding of $CO_2$ to vanadium, forming surface $CO_2$-species, resulting in the formation of vanadyl groups and CO. In this context, it is worth mentioning that, according to DFT results for $VO_x/SiO_2$ by Rozanska et al. [52], $N_2O$ is not able to re-oxidize V(+4) sites, a result which might be transferable to $CO_2$. Based on these literature findings, it appears reasonable that re-oxidation of reduced vanadia occurs via $CO_2$ adsorption on $V^{3+}$ and recovery of the vanadyl bond, accompanied by CO formation. Considering recent work on re-oxidation of reduced $VO_x$ by $CO_2$, this process is expected to be slow on the timescale of the *operando* experiment. [25,27] As a consequence, the vanadyl signal shows a decreased intensity during propane ODH with $CO_2$ in comparison to the signal after $CO_2$ re-oxidation (see Figure 2). In contrast, during propane DH, a highly reduced vanadia catalyst is formed, showing a different spectroscopic signature (see Figure 4). Thus, we can rule out the occurrence of ODH in parallel to DH (without further oxidation). Besides, $CO_2$ treatment after propane DH was able to largely re-oxidize vanadyl (not shown). In fact, our

*operando* spectroscopic findings are fully consistent with the parallel occurrence of both pathways, i.e., direct ODH (one step) and dehydrogenation followed by a reverse water-gas shift reaction (two step).

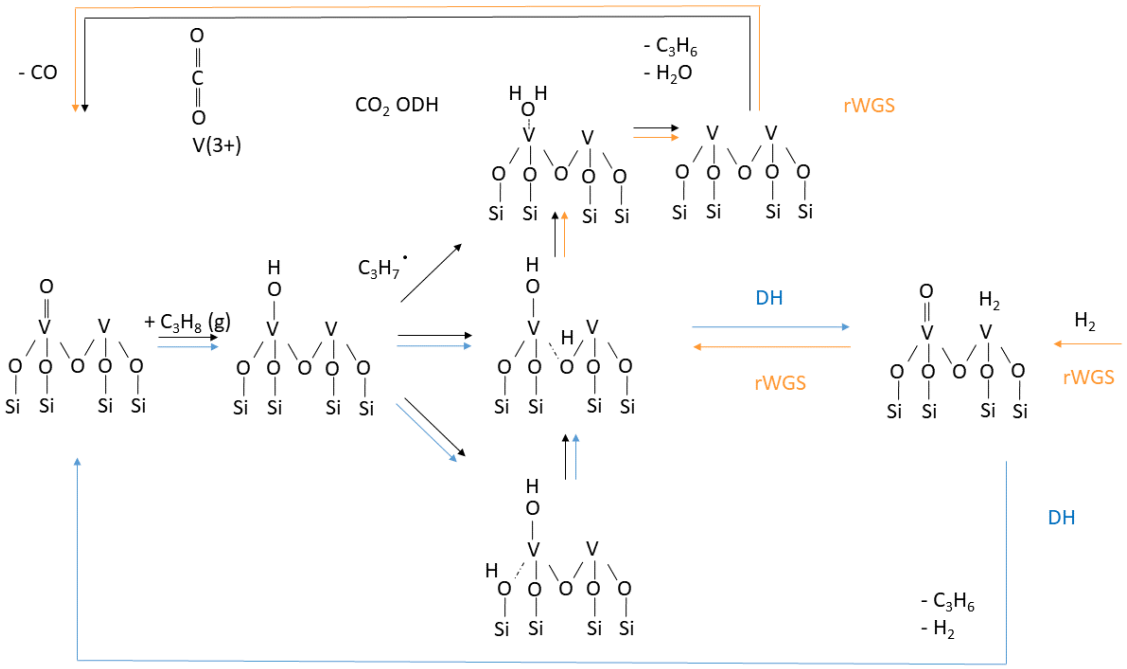


**Figure 5.** Proposed reaction mechanism for propane ODH with $CO_2$ over $VO_x/SiO_2$ catalysts.

Theoretical modelling by Ascoop et al. assumed V-O-V bridging oxygen of dimers to be responsible for the second H-abstraction from the initially formed propyl radical. [27] The presence of dimers/small oligomers is in agreement with our *operando* results. During reaction conditions, the amount of V-O-V decreased compared to the oxidized state (see bottom of Figure 2), pointing to a decrease in the degree of oligomerization. These structural changes are proposed to be accompanied by the attachment of hydrogen atoms to vanadyl. Moreover, the presence of hydrogen in the reduced/reactive states of the catalyst surface was evidenced spectroscopically by the detection of silanol groups (SiO-H), indicating the breakage of V-O-Si bond [53].

## 4. Conclusions

A detailed understanding of propane ODH is of academic and industrial interest. To gain direct mechanistic insight into propane ODH over $VO_x/SiO_2$ catalysts using $CO_2$ as mild oxidant we employed *operando* Raman spectroscopy. We demonstrate the sensitivity of UV Raman spectroscopy to monitor the structural dynamics of the surface vanadia as a function of gas-phase composition and to provide mechanistic information on the overall propane ODH reaction network.

Switching from oxidizing to reducing/reaction conditions affects V=O, V-O-V and V-O-Si bonds, whose oxygen atoms are responsible for the hydrogen abstraction during the reaction. Under reaction conditions, we observe mainly dimeric/small oligomeric vanadia species with part of the vanadyl reduced, which may support the increased selectivity by limiting the amount of oxygen inducing deep oxidation. Using $CO_2$, vanadyl can be re-oxidized to the state prior reaction.

In comparison to propane ODH, during propane DH conditions the presence of carbon deposits and higher degree of reduction is observed, while the *operando* signature of the rWGS reaction rather resembles that of propane ODH. As $CO_2$ is shown to enable vanadyl oxidation, our *operando* results are fully consistent with the occurrence of two parallel pathways, i.e., direct ODH (one step) and dehydrogenation followed by a reverse water-gas shift reaction (two step).

## Acknowledgements

The authors thank Karl Kopp for technical support and Silvio Heinschke for BET measurements. Leon Schumacher and Martin Lucas are gratefully acknowledged for their work and technical support regarding the GC/Raman setup. This work was supported by the Deutsche Forschungsgemeinschaft (DFG, HE 4515/11-1).

## References


[1] J. Bricker, History and State of the Art of Ethane/Propane Dehydrogenation Catalysis., Washington, DC, 2016.

[2] F. Cavani, N. Ballarini, A. Cericola, Oxidative dehydrogenation of ethane and propane: How far from commercial implementation?, Catal. Today 127 (2007) 113–131. https://doi.org/10.1016/j.cattod.2007.05.009.

[3] C.A. Carrero, R. Schloegl, I.E. Wachs, R. Schomaecker, Critical Literature Review of the Kinetics for the Oxidative Dehydrogenation of Propane over Well-Defined Supported Vanadium Oxide Catalysts, ACS Catal. 4 (2014) 3357–3380. https://doi.org/10.1021/cs5003417.

[4] M. Aresta, A. Dibenedetto, Utilisation of $CO_2$ as a chemical feedstock: Opportunities and challenges, Dalton Trans. (2007) 2975–2992. https://doi.org/10.1039/b700658f.

[5] M. Aresta, A. Dibenedetto, A. Angelini, The changing paradigm in $CO_2$ utilization, J. $CO_2$ Util. 3-4 (2013) 65–73. https://doi.org/10.1016/j.jcou.2013.08.001.

[6] K.M.K. Yu, I. Curcic, J. Gabriel, S.C.E. Tsang, Recent advances in $CO_2$ capture and utilization, ChemSusChem 1 (2008) 893–899. https://doi.org/10.1002/cssc.200800169.

[7] M.B. Ansari, S.-E. Park, Carbon dioxide utilization as a soft oxidant and promoter in catalysis, Energy Environ. Sci. 5 (2012) 9419. https://doi.org/10.1039/c2ee22409g.

[8] G. Raju, B.M. Reddy, S.-E. Park, Utilization of carbon dioxide in oxidative dehydrogenation reactions, Indian J. Chem. (2012).

[9] S. Kawi, Y. Kathiraser, $CO_2$ as an Oxidant for High-Temperature Reactions, Front. Energy Res. 3 (2015) 21. https://doi.org/10.3389/fenrg.2015.00013.

[10] M.A. Atanga, F. Rezaei, A. Jawad, M. Fitch, A.A. Rownaghi, Oxidative dehydrogenation of propane to propylene with carbon dioxide, Appl. Catal. B 220 (2018) 429–445. https://doi.org/10.1016/j.apcatb.2017.08.052.

[11] S.T. Rahman, J.-R. Choi, J.-H. Lee, S.-J. Park, The Role of $CO_2$ as a Mild Oxidant in Oxidation and Dehydrogenation over Catalysts: A Review, Catalysts 10 (2020) 1075. https://doi.org/10.3390/catal10091075.

[12] E. Gomez, B. Yan, S. Kattel, J.G. Chen, Carbon dioxide reduction in tandem with light-alkane dehydrogenation, Nat Rev Chem 3 (2019) 638–649. https://doi.org/10.1038/s41570-019-0128-9.

[13] D. Mukherjee, S.-E. Park, B.M. Reddy, $CO_2$ as a soft oxidant for oxidative dehydrogenation reaction: An eco benign process for industry, J. $CO_2$ Util. 16 (2016) 301–312. https://doi.org/10.1016/j.jcou.2016.08.005.

[14] P. Michorczyk, J. Ogonowski, Dehydrogenation of propane in the presence of carbon dioxide over oxide-based catalysts, React. Kinet. Catal. Lett. 78 (2003) 41–47. https://doi.org/10.1023/A:1022501613772.

[15] P. Michorczyk, J. Ogonowski, P. Kuśtrowski, L. Chmielarz, Chromium oxide supported on MCM-41 as a highly active and selective catalyst for dehydrogenation of propane with $CO_2$, Appl. Catal. A 349 (2008) 62–69. https://doi.org/10.1016/j.apcata.2008.07.008.

[16] P. Michorczyk, J. Ogonowski, M. Niemczyk, Investigation of catalytic activity of CrSBA-1 materials obtained by direct method in the dehydrogenation of propane with $CO_2$, Appl. Catal. A 374 (2010) 142–149. https://doi.org/10.1016/j.apcata.2009.11.040.

[17] P. Michorczyk, J. Ogonowski, K. Zeńczak, Activity of chromium oxide deposited on different silica supports in the dehydrogenation of propane with $CO_2$ – A comparative study, J. Mol. Catal. A: Chem. 349 (2011) 1–12. https://doi.org/10.1016/j.molcata.2011.08.019.

[18] P. Michorczyk, P. Pietrzyk, J. Ogonowski, Preparation and characterization of SBA-1–supported chromium oxide catalysts for $CO_2$ assisted dehydrogenation of propane, Microporous Mesoporous Mater. 161 (2012) 56–66. https://doi.org/10.1016/j.micromeso.2012.05.011.

[19] J. Baek, H.J. Yun, D. Yun, Y. Choi, J. Yi, Preparation of Highly Dispersed Chromium Oxide Catalysts Supported on Mesoporous Silica for the Oxidative Dehydrogenation of Propane Using $CO_2$ Insight into the Nature of Catalytically Active Chromium Sites, ACS Catal. 2 (2012) 1893–1903. https://doi.org/10.1021/cs300198u.

[20] T. Shishido, K. Shimamura, K. Teramura, T. Tanaka, Role of $CO_2$ in dehydrogenation of propane over Cr-based catalysts, Catal. Today 185 (2012) 151–156. https://doi.org/10.1016/j.cattod.2011.10.028.

[21] I. Takahara, M. Saito, M. Inaba, K. Murata, Dehydrogenation of propane over a silica-supported vanadium oxide catalyst, Catal. Lett. 102 (2005) 201–205. https://doi.org/10.1007/s10562-005-5856-4.

[22] K. Nakagawa, C. Kajita, N.-o. Ikenaga, M. Nishitani-Gamo, T. Ando, T. Suzuki, Dehydrogenation of light alkanes over oxidized diamond-supported catalysts in the

presence of carbon dioxide, Catal. Today 84 (2003) 149–157. https://doi.org/10.1016/S0920-5861(03)00268-2.

[23] A.S. Sandupatla, K. Ray, P. Thaosen, C. Sivananda, G. Deo, Oxidative dehydrogenation of propane over alumina supported vanadia catalyst – Effect of carbon dioxide and secondary surface metal oxide additive, Catal. Today (2019). https://doi.org/10.1016/j.cattod.2019.06.047.

[24] M.L. Balogun, S. Adamu, M.S. Ba-Shammakh, M.M. Hossain, Promotional effects of $CO_2$ on the oxidative dehydrogenation of propane over mesoporous $VO_X/\gamma Al_2O_3$ catalysts, J. Ind. Eng. Chem. 96 (2021) 82–97. https://doi.org/10.1016/j.jiec.2020.12.022.

[25] P. Djinović, J. Zavašnik, J. Teržan, I. Jerman, Role of $CO_2$ During Oxidative Dehydrogenation of Propane Over Bulk and Activated-Carbon Supported Cerium and Vanadium Based Catalysts, Catal. Lett. (2021). https://doi.org/10.1007/s10562-020-03519-y.

[26] E. Nowicka, C. Reece, S.M. Althahban, K.M.H. Mohammed, S.A. Kondrat, D.J. Morgan, Q. He, D.J. Willock, S. Golunski, C.J. Kiely, G.J. Hutchings, Elucidating the Role of $CO_2$ in the Soft Oxidative Dehydrogenation of Propane over Ceria-Based Catalysts, ACS Catal. 8 (2018) 3454–3468. https://doi.org/10.1021/acscatal.7b03805.

[27] I. Ascoop, V.V. Galvita, K. Alexopoulos, M.-F. Reyniers, P. van der Voort, V. Bliznuk, G.B. Marin, The role of $CO_2$ in the dehydrogenation of propane over $WO_x$–$VO_x/SiO_2$, J. Catal. 335 (2016) 1–10. https://doi.org/10.1016/j.jcat.2015.12.015.

[28] A. Brückner, Monitoring transition metal ions (TMI) in oxide catalysts during (re)action: The power of operando EPR, Phys. Chem. Chem. Phys. 5 (2003) 4461–4472. https://doi.org/10.1039/B305884K.

[29] G. Mul, M.A. Bañares, G. Garcia Cortéz, B. van der Linden, S.J. Khatib, J.A. Moulijn, MultiTRACK and operando Raman-GC study of oxidative dehydrogenation of propane over alumina-supported vanadium oxide catalysts, Phys. Chem. Chem. Phys. 5 (2003) 4378–4383. https://doi.org/10.1039/B305813C.

[30] A. Brückner, Killing three birds with one stone--simultaneous operando EPR/UV-vis/Raman spectroscopy for monitoring catalytic reactions, Chem. Commun. 0 (2005) 1761–1763. https://doi.org/10.1039/B418790C.

[31] A.M. Beale, A.M.J. van der Eerden, K. Kervinen, M.A. Newton, B.M. Weckhuysen, Adding a third dimension to operando spectroscopy: a combined UV-Vis, Raman and XAFS setup to study heterogeneous catalysts under working conditions, Chem. Commun. (2005) 3015–3017. https://doi.org/10.1039/b504027b.

[32] M.V. Martínez-Huerta, G. Deo, J.L.G. Fierro, M.A. Bañares, Operando Raman-GC Study on the Structure−Activity Relationships in $V^{5+}/CeO_2$ Catalyst for Ethane Oxidative Dehydrogenation: The Formation of $CeVO_4$, J. Phys. Chem. C 112 (2008) 11441–11447. https://doi.org/10.1021/jp802827t.

[33] P. Waleska, S. Rupp, C. Hess, *Operando* Multiwavelength and Time-Resolved Raman Spectroscopy: Structural Dynamics of a Supported Vanadia Catalyst at Work, J. Phys. Chem. C 122 (2018) 3386–3400. https://doi.org/10.1021/acs.jpcc.7b10518.

[34] P. Ober, S. Rogg, C. Hess, Direct Evidence for Active Support Participation in Oxide Catalysis: Multiple Operando Spectroscopy of $VO_x$/Ceria, ACS Catal. 10 (2020) 2999–3008. https://doi.org/10.1021/acscatal.9b05174.

[35] L. Schumacher, C. Hess, The active role of the support in propane ODH over $VO_x/CeO_2$ catalysts studied using multiple operando spectroscopies, J. Catal. 398 (2021) 29–43. https://doi.org/10.1016/j.jcat.2021.04.006.

[36] C. Hess, New advances in using Raman spectroscopy for the characterization of catalysts and catalytic reactions, Chem. Soc. Rev. 50 (2021) 3519–3564. https://doi.org/10.1039/d0cs01059f.

[37] S. Jin, Z. Feng, F. Fan, C. Li, UV Raman Spectroscopic Characterization of Catalysts and Catalytic Active Sites, Catal. Lett. 145 (2015) 468–481. https://doi.org/10.1007/s10562-014-1416-0.

[38] H. Kim, K.M. Kosuda, Van Duyne, Richard P., P.C. Stair, Resonance Raman and surface- and tip-enhanced Raman spectroscopy methods to study solid catalysts and heterogeneous catalytic reactions, Chem. Soc. Rev. 39 (2010) 4820–4844. https://doi.org/10.1039/c0cs00044b.

[39] J.P. Thielemann, F. Girgsdies, R. Schlögl, C. Hess, Pore structure and surface area of silica SBA-15: Influence of washing and scale-up, Beilstein J. Nanotechnol. 2 (2011) 110–118. https://doi.org/10.3762/bjnano.2.13.

[40] P. Ruff, S. Lauterbach, H.-J. Kleebe, C. Hess, Surface structuring of mesoporous materials by controlled synthesis of nanocavities, Microporous Mesoporous Mater. 235 (2016) 160–169. https://doi.org/10.1016/j.micromeso.2016.08.005.

[41] G.H. Vogel, G. Kaibel, Verfahrensentwicklung: Von der ersten Idee zur chemischen Produktionsanlage, Wiley-VCH, Weinheim, 2007.

[42] A. Filtschew, C. Hess, Unravelling the mechanism of NO and $NO_2$ storage in ceria: The role of defects and Ce-O surface sites, App. Catal. B 237 (2018) 1066–1081. https://doi.org/10.1016/j.apcatb.2018.06.058.

[43] P.S. Waleska, C. Hess, Oligomerization of Supported Vanadia: Structural Insight Using Surface-Science Models with Chemical Complexity, J. Phys. Chem. C 120 (2016) 18510–18519. https://doi.org/10.1021/acs.jpcc.6b01672.

[44] H.E. Howard-Lock, B.P. Stoicheff, Raman intensity measurements of the Fermi diad $\nu_1$, $2\nu_2$ in $^{12}CO_2$ and $^{13}CO_2$, J. Mol. Spectrosc. 37 (1971) 321–326. https://doi.org/10.1016/0022-2852(71)90302-X.

[45] D. Nitsche, C. Hess, Structure of Isolated Vanadia and Titania: A Deep UV Raman, UV–Vis, and IR Spectroscopic Study, J. Phys. Chem. C 120 (2016) 1025–1037. https://doi.org/10.1021/acs.jpcc.5b10317.

[46] L. Abello, E. Husson, Y. Repelin, G. Lucazeau, Structural study of gels of $V_2O_5$: Vibrational spectra of xerogels, J. Solid State Chem. 56 (1985) 379–389. https://doi.org/10.1016/0022-4596(85)90188-4.

[47] F.D. Hardcastle, I.E. Wachs, Determination of vanadium-oxygen bond distances and bond orders by Raman spectroscopy, J. Phys. Chem. 95 (1991) 5031–5041. https://doi.org/10.1021/j100166a025.

[48] Z. Wu, S. Dai, S.H. Overbury, Multiwavelength Raman Spectroscopic Study of Silica-Supported Vanadium Oxide Catalysts, J. Phys. Chem. C 114 (2009) 412–422. https://doi.org/10.1021/jp9084876.

[49] A.C. Ferrari, Raman spectroscopy of graphene and graphite: Disorder, electron–phonon coupling, doping and nonadiabatic effects, Solid State Commun. 143 (2007) 47–57. https://doi.org/10.1016/j.ssc.2007.03.052.

[50] C. Li, P.C. Stair, Ultraviolet Raman spectroscopy characterization of coke formation in zeolites, Catal. Today 33 (1997) 353–360.

[51] M.A. Haija, Y. Romanyshyn, A. Uhl, H. Kuhlenbeck, H.-J. Freund, Carbon Dioxide Adsorption on $V_2O_3$(0001), Top. Catal. 60 (2017) 413–419. https://doi.org/10.1007/s11244-017-0810-4.

[52] X. Rozanska, E. Kontratenko, J. Sauer, Oxidative dehydrogenation of propane: Differences between $N_2O$ and $O_2$ in the reoxidation of reduced vanadia sites and consequences for selectivity, J. Catal. 256 (2008) 84–94. https://doi.org/10.1016/j.jcat.2008.03.002.

[53] X. Rozanska, R. Fortrie, J. Sauer, Oxidative Dehydrogenation of Propane by Monomeric Vanadium Oxide Sites on Silica Support, J. Phys. Chem. C 111 (2007) 6041–6050. https://doi.org/10.1021/jp071409e.

**TOC graphic**

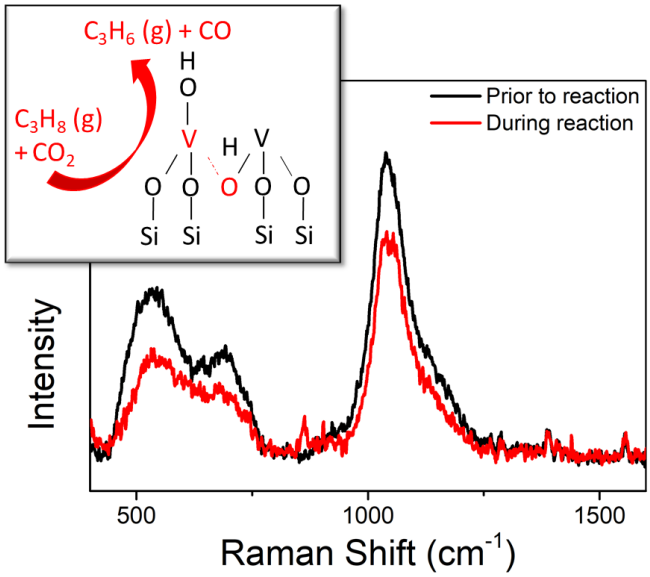
C3H6 (g) + CO
C3H8 (g)
+ CO2
H
O
V
H
V
O
O
O
O
O
Si
Si
Si
Si
Prior to reaction
During reaction
Intensity
500
1000
1500
Raman Shift (cm-1)